Damping of Plasmons of Closely-Coupled Sphere Chains due to Disordered Gaps

Mathias S. Scheurer[1,2], *Matthew D. Arnold*[1*], *Jeffry Setiadi*[1], *Michael J. Ford*[1]

[1] School of Physics and Advanced Materials, University of Technology Sydney, PO Box 123, Broadway NSW 2007, Australia.

[2] visiting from Fakultät für Physik, Karlsruhe Institute of Technology, 76128 Karlsruhe, Germany

* Corresponding author: matthew.arnold-1@uts.edu.au

ph: +61 2 9514 9715

fax: +61 2 9514 2219

Abstract: The damping of plasmons due to structural disorder may have important practical consequences. Here we use spherical harmonic expansions to quantify the damping of plasmons of ensembles of closely coupled sphere chains with moderately disordered gaps. We show that the quadratic shift of average resonance position due to disorder is maintained in the transition from weak to close coupling, but the sensitivity to disorder increases. Further we find that although the main peak is most often damped and broadened by disorder, it is possible for the optical extinction of disordered gold chains to increase slightly due to red-skew into a region with more favorable metal properties.

Keywords: electrostatic resonance, optical extinction, off-diagonal coupling, dipole mode

Introduction

Plasmonic resonances strongly concentrate electromagnetic fields, which can be exploited in a range of applications including those involving energy transport[1,2], imaging[3,4], and sensing[5,6]. The damping of plasmonic resonances usually reduces their performance in applications and understanding this problem is of considerable practical importance. Damping mechanisms range from large-scale mechanisms such as radiative damping, to small-scale quantum mechanisms[7-9]. In between these two extremes the performance can be maximized within the limitations of the materials and fabrication techniques. The choice of material is quite important because the quality of plasmons is related to the ratio of the real and imaginary parts of the permittivity[10,11]. Most often, however, practical constraints dictate the material used – the alkalis have the lowest loss and hence excellent plasmonic quality, but gold is used in the majority of cases because it is chemically inert even though its optical performance is somewhat inferior. Given a particular material, the performance can be optimized by varying the geometry to align the resonance with the optimum frequency for the material. To some extent, depending upon the particular method used to synthesize a nanostructure, disorder will always be present leading to damping independent of the material properties. It is therefore important to understand how disorder affects the plasmonic performance and more importantly how tolerant to disorder this performance will be.

Some types of disordered plasmonic structures have been studied extensively, such as random composites[12], however in this article our focus is on simple structures with only moderate disorder due to fabrication tolerances. In particular, previous investigations have considered only some aspects of the effect of moderate disorder on loosely coupled sphere arrays, including fundamental scalings of quasistatic modes[13], reduced damping of non-quasistatic modes[14], and the effect of disorder on diffractive modes[15]. As the system can be considered in terms of a matrix describing interactions of spheres, the disorder can be

classified as being “diagonal” or “off-diagonal”. Diagonal disorder corresponds to variations in the self-interaction of each sphere due to variations in composition or size. Although this type of disorder is a possible result of fabrication variations, we are more interested in off-diagonal disorder which is due to variations in coupling between particles. Variation in the gap between particles is expected to have a strong effect due to the concentration of the field in that region. Previously a dipole model was used to find a fundamental scaling of off-diagonal disorder that applies to weakly coupled quasistatic modes[13]. In this article we will consider the effect of disorder on the longitudinal resonances of sphere chains due to variations in the interparticle spacing, and in particular systematically consider the effect of close coupling and compare the relative sensitivities of common plasmonic materials. This system is a coupled nanostructure[16] that is relatively simple, but allows very strong enhancement and exhibits multipole resonances even in the small-scale electrostatic limit. Previously we reviewed the applications and plasmonic properties of ordered sphere chains[17]. In particular, we showed how to exploit the separability of geometry and material properties to simplify the optimization of resonances for various metals.

Methods

The various shape parameters for the sphere chains considered here are represented in Figure 1. This is a one-dimensional chain of N spheres each with identical radius a, and separated by a gap g. The centre to centre spacing of the spheres is therefore $d=g+2a$. The gap fraction is defined as $f=g/2a$. The plane-wave incident vector k is small enough that retardation can be ignored, such that $kd<<1$, and the electric field E excites the chain longitudinally.

Disorder is introduced into the chain geometry by varying the interparticle gap. The disorder is characterized by statistical distributions about the mean (ordered) positions.

Gaussian (normal) statistics, with a deviation σ, were used because they are well understood and physically relevant to some fabrication processes. This also gives us a relatively simple and consistent way to characterize the degree of disorder introduced into the chain spacings in terms of the ratio σ/g of the standard deviation of statistical spread of gap sizes to the ordered gap size. As this parameter increases in magnitude, the degree of disorder increases. However to ensure physically valid results and limit calculation time it is necessary to maintain positive inter-particle gaps which necessarily truncates the distribution. Ultimately we limited the standard deviation σ so that the truncation was statistically insignificant. As expected a significant number of samples were required to ensure smooth statistics – we used 10^4 samples for most of our results. The sample statistics of the ensembles were then calculated; however it is important to keep in mind throughout the analysis that an individual configuration could be quite different from the mean.

Calculating the modes of the close-coupling regime requires a numerical technique that accurately samples the near-fields, especially in the rapidly varying gap region. Due to spherical geometry, multipole spherical harmonics expansions are relatively efficient and can be used to find the mode parameters directly[18]. The eigenmodes are described by the eigenvalues S and the eigenvectors ψ that are solutions to the usual eigenvalue problem

$$H\psi = S\psi . \tag{1}$$

The spherical harmonic basis used in this article describes eigenvectors ψ in terms of multipole moments numbered l on each sphere numbered n, with a Hermitian interaction matrix H that has off-diagonal blocks

$$H_{nn'} = \left(\frac{a}{d_{nn'}}\right)^{l+l'+1} \frac{n-n'}{|n-n'|}(-1)^{l'} \sqrt{\frac{ll'}{(2l+1)(2l'+1)}} \prod_{p=1}^{l'}\left(1+\frac{1}{p}\right), \tag{2}$$

and diagonal blocks

$$H_{nn} = \delta_{ll'} \frac{l}{2l+1} \ . \tag{3}$$

We have rewritten the factorials usually used in Eq (2) to avoid numerical overflow. More importantly, we have restricted our investigation to disorder along the chain to maintain azimuthal symmetry so that only the fundamental azimuthal mode (m=0) is required, which greatly increases numerical efficiency. It is important to consider both the effect of the number of particles N and the number of orders retained (l=1...L). Most of our results are based around N=9, which is less expensive than a long chain but relatively similar in behavior. The time taken to diagonalize the interaction matrix goes as $(NL)^3$, which must be balanced against large L required for accuracy. We used the convergence of two spheres to estimate the required number of orders

$$L = -\log_{10}(\xi)/\sqrt{f} \tag{4}$$

at a given tolerance (ξ=10^{-6}) and gap fraction f.

In order to compare mode parameters to a physically measureable quantity we will calculate the spectrum of the extinction cross-section C_e, which describes the relative power flux that is diverted due to scattering and absorption. One way to solve this is to calculate the electric fields by adding a plane-wave excitation, where a direct interpretation would imply expensive numerical inversion at each frequency of interest. However, this can easily be rewritten as a weighted sum over modes. In the electrostatic limit it can be shown that the observable far-field properties are determined by the dipole moment, and in particular the extinction C_e may be expressed as

$$C_e = kV \,\mathrm{Im}\left\{ \sum_{j=1}^{LN} \frac{A_j}{S_j - s} \right\} , \tag{5}$$

where $s = 1/(1-\varepsilon)$ is a continuous function of permittivity ratio ε, k is the corresponding wave-vector, and V is the total volume of the spheres, and the sum is performed over the

geometry-dependent modes. In our spherical harmonic basis, the eigenvalues S_j appear directly, and A_j are the corresponding weights given by the square of the net dipole moment [19]. Explicitly, the weighting due to uniform excitation is given by

$$A_j = \left| \sum_{n=1}^{N} \psi_{(n,l=1),j} \right|^2 . \tag{6}$$

Mode parameters are independent of material: once they have been calculated for a particular geometry, Eq (5) can be applied to any chosen material with minimal effort. We verified the resulting extinction against a public domain vector spherical harmonic (VSH) code[20], which we had previously tested against a range of other methods. The calculations presented here are electrostatic (non-retarded), however we have previously shown that despite a systematic shift due to retardation, the relative scaling is very similar[17] so retardation can be ignored.

We will now briefly discuss the expected mode parameters and some implications. In our choice of basis the eigenvalues can be identified as depolarizations, which must lie in the range $0<S<1$; specifically isolated spheres start from $S=1/3$ and coupling breaks degeneracy of collective modes causing splitting in the red (small) and blue (large) wavelength directions. Mode weights lie in the range $0<A<1$, and are constrained by the sum rule $\Sigma A=1$. Chains of spheres have a mode scaling that depends weakly on the number of spheres N but very strongly on the ratio between the sphere size a and the gap g between them[21]. Coupling increases with decreasing gap fraction $f=g/2a$, resulting in a strong red-shift of the dipole and increasing contribution of higher order modes. With this knowledge it is easy to predict the behavior of any material and identify the optimum geometry. For many common plasmonic materials, interband transitions lie near the plasma frequency which means the optimum is considerably red-shifted requiring quite small gaps compared to the particle size[17].

Unfortunately this regime is most susceptible to fabrication anomalies, and so it is important to quantify the associated damping effect.

Results and Discussion

We first present here our ensemble results in terms of the depolarization factors S and weights A of Eq (5) for the three lowest modes (j=1,2,3). The weight for each mode represents its spectral strength, while the depolarization determines the mode position in wavelength. Plotting the (considerable) amount of data in this way is a convenient way to display the statistical variation. It also allows us to demonstrate the effect of disorder independent of material properties. Figure 2 shows how the mode strengths and positions spread in response to disorder in the interparticle gap.

The dominant mode is typically the collective dipole mode (j=1) which has the lowest frequency and thus red-shifts the most (its depolarization decreases). This occurs because narrower gaps red-shift the dipole and they make a stronger contribution to polarization than wider gaps so the net response is skewed to the red. Disorder weakens this mode compared to the ordered chain due to reduction in symmetry. Conversely, the even modes increase in strength because strict anti-symmetry is broken resulting in a net dipole moment: for the ordered chain these modes have zero weight as can be seen by the j=2 mode in Figure 2.

Now that we have the calculated mode weights and depolarizations (such as those shown in Figure 2), the extinction spectra for a particular material can be calculated from the corresponding dielectric function and Eq (5). Figure 3 shows an example of this for potassium spheres where the bulk dielectric function interpolated from experimental tables is used[22]. There is a definite damping of the ensemble average compared to the ordered response. Some additional damping would be expected at strong coupling due to non-local effects[8]. We will return to the effect of material properties in more detail later where we will

compare four representative high quality metals based on either common usage in plasmonics (Au, Ag), unusual behavior (Al), or very low losses (K). We now detail the effect of disorder on mode scaling, concentrating on the collective dipole (j=1) mode. As noted earlier, our discussion is considerably simplified by ignoring retardation - Figure 4 shows that this simplification has little effect on the scaling of the mode shift.

Figure 5 shows how the various mode parameters relate to disorder σ and gap fraction f. The average shift of the depolarization (mode position) $\langle \delta S \rangle$ for varying disorder is proportional to σ^2 across the entire range of coupling strengths (Figure 5a). Although not shown here, the lowest modes all have a similar shift albeit with some subtle variation. Perhaps not surprisingly the shift is also larger at closer coupling, however it does not vary as dramatically as the eigenvalue itself. Figure 5b shows that with disorder ratio (σ/g) fixed the red-shift decreases as the gap fraction is increased, and analysis of the data shows that it varies approximately exponentially at strong coupling (f<1) according to the expression

$$\langle \delta S \rangle / S \sim (\sigma / g)^2 \exp(-f), \tag{7}$$

but for weak coupling scales more like

$$\langle \delta S \rangle / S \sim 6(\sigma / g)^2 f^{-3}. \tag{8}$$

There is no obvious quantitative explanation for the strong-coupling result, but the weak coupling result is perhaps not surprising given the scaling of the ordered chain shown in previous work[17]. These tentative models have been overlaid on Figure 5b. As discussed below, it is relatively difficult to predict these results analytically, but the main result of reduced red-shifting with decreasing coupling is still useful. The data also shows how the dipole mode is damped in response to disorder – naturally increasing disorder has a stronger damping effect (Figure 5c), but relative damping as measured by $-\langle \delta A \rangle / A$ decreases in magnitude with increasing coupling (Figure 5d).

Higher order statistics of the disordered modes are required for a full description of the observed behavior, and so the standard deviation and skewness of the mode position and strength are shown in Figure 6. It is important to understand that the standard deviation is typically larger than the mean shift, as can be observed by comparing Figure 6a to Figure 5a. Further, Figure 6b shows that the shift is skewed and that this increases with disorder. The strength of the modes also have significant standard deviation (Figure 6c). Although not shown here, there are some differences in the strength of different modes because even modes start from zero strength. The dipole mode is unique in that it is skewed towards reduced strength (Figure 6d) – all other modes skew towards increasing strength, especially the even modes which are zero in the ordered chain and therefore have skew nearly independent of disorder. Kurtosis is also evident in the mode parameters but this has similar origin to the skew. In short, the distributions are both wide and strongly skewed which should be considered when interpreting mean results.

The effect of disorder σ can be modeled using perturbation theory. Assuming that a disordered interaction matrix is perturbed by δH compared to the ordered case, the perturbation of the eigenvalues to second order is approximated by

$$\delta S_j \approx \langle \Psi_j | \delta H | \Psi_j \rangle + \sum_{k \neq j} \frac{\left| \langle \Psi_k | \delta H | \Psi_j \rangle \right|^2}{S_j - S_k} + O(\delta H^3). \tag{9}$$

Previously, the average of the perturbed eigenvalue to first order was estimated using the analytical average of nearest-diagonals of δH, yielding the correct σ^2 dependence[13]. However the coefficient found does not match full numerical results and this approach cannot be reliably extended to higher orders. We found it impractical to calculate the full perturbation analytically, but some insight can be gained by considering how the various parts contribute, which can be confirmed numerically (Figure 7). It can be shown that both first and second order perturbation have σ^2 dependence for the strongest terms, while third

order and above only require σ^4 so can be neglected for most practical purposes (as seen in Figure 7b). Second order terms strictly require the calculation of covariances between the elements of the interaction matrix. This is relatively expensive to calculate but is dominated by nearest-neighbor interactions. It is also interesting that the most significant contributions come from correlated movements where at least one of the particle movements is due to the same particle (i.e. two- or three- body rather than a four-body correlation). This explains why the second order makes a significant contribution to the perturbation (Figure 7a). These results are consistent with the observation that progressively adding particles to the chain makes progressively less difference after three particles – that is, nearest-neighbor interactions dominate but both nearest-neighbors of a particle are important.

We turn now to the extinction described by Eq (5), which provides an experimentally-relevant measure of the contribution of all modes. In particular, we focus on the main peak which predominantly results from the j=1 mode, and measure the maximum extinction, the wavelength at which this occurs, and the full-width-half-maximum (FWHM). Unlike previous figures, these results derived from extinction depend on the permittivity[22] for the four metals selected (Ag, Al, Au, K).

Firstly, Figure 8 shows the average relative shift of the peak wavelength λ_p. The red-shift of the peak is relatively small, which means that experimental resonances would not be expected to move very much in wavelength. It should be noted that the shift for nearly ideal metals such as K (Figure 8d) is larger than that of Au (Figure 8c), because Au has a relatively flat real permittivity due to the close proximity of a relatively strong absorption band. Nevertheless, all metals tested here exhibit increasing shift with both increasing disorder and increasing coupling, consistent with the general observation that the resonances are more sensitive to gap changes when the gaps are small.

Further, Figure 9 shows how the FHWM (labeled Δ_p) is affected by disorder. In this case disorder has more effect, but once again the response of Au (Figure 9c) is substantially different compared with other metals due to its unusual permittivity function. The other metals show some broadening around moderate coupling. It is important to understand that generally a peak associated with a well-distinguished mode would not necessarily broaden[17], even though its magnitude may be decreased due to redistribution to other well-distinguished modes. In the case shown in Figure 9, other nearby modes are contributing to the extinction around the main peak – in particular the adjacent j=2 mode increases in magnitude with disorder (see Figure 2 for example). The effect on the main peak is most pronounced at moderate coupling, because at weak coupling the additional modes have low strength, and at strong coupling they have less influence due to better spectral separation. Additionally we have included an estimate of the broadening of an ensemble of chains (dashed lines), where notably there is a further increase in broadening for K at strong coupling (Figure 9d) due to comparatively larger smearing of the peak position.

The most important experimental evidence of damping is the change in peak extinction (labeled C_p) shown in Figure 10. It is notable that the maximum extinction of some disordered chains exceeds similar ordered chains by a small margin (about 1%), most noticeably for gold spheres near gap-fraction f=0.5 (see Figure 10c), but also to a lesser extent for Ag near f=2 (Figure 10a). Although the strength of the dominant dipole mode declines with disorder, it does so slowly, and the other modes spread to replace it. Further, many metals (with the notable exception of aluminum) exhibit reduced loss with red-shift, which is the reason that extinction usually increases as the coupling is increased[17]. A practical consequence is that the strength of plasmons of gold spheres chains is relatively robust against positional variation. However, because alkalis are nearly ideal metals, their loss reduces relatively weakly with red-shift and the high quality modes are more sensitive to

variation, so they are noticeably less robust (Figure 10d), as are those of Al (Figure 10b). The peak ensemble extinction (dashed) for K shows additional damping at strong coupling due to smearing of the peak positions.

A final comment is that damping of the delocalized chain plasmon is associated with localization[13], which is a subject of considerable interest. The practical consequence is that the polarization and hence electric field is greatly enhanced around particular gaps, which is particularly useful for sensing techniques such as SERS. It would be interesting to investigate the field enhancements in this system, however doing so would require considerable computational resources and would need to be compared critically to the enhancement of higher order multipoles. Additionally, it is expected that the electric field would be quite strongly affected by non-local effects[23].

Conclusion

In conclusion, we have investigated the effect of moderate gap disorder on electrostatic resonances sphere chains, and found that quadratic scaling of the average dipole shift extends into the close-coupling regime. Increased coupling increases the sensitivity to disorder. The distribution of optical response is significantly skewed compared to the structural distribution, which is expected due to higher sensitivity to narrowing than widening gaps. We find that perturbation analysis should be approached carefully because second order terms are significant, and although analysis of higher order terms confirms that mode shift is quadratic with disorder, estimating the average effect of coupling from configuration statistics is impractical and instead requires averaging individual configurations. When considering how optical extinction would be affected by the metal used, we find the average extinction of chains composed of reasonably ideal metals such as K is damped significantly

by disorder, but poorer metals such as Au are surprisingly resilient to disorder and can be slightly enhanced at moderate coupling.

References

(1) Giannini, V.; Fernandez-Dominguez, A. I.; Heck, S. C.; Maier, S. A. *Chem Rev* **2011**, *111*, 3888-3912.

(2) Denisyuk, A. I.; Adamo, G.; MacDonald, K. F.; Edgar, J.; Arnold, M. D.; Myroshnychenko, V.; Ford, M. J.; de Abajo, F. J. G.; Zheludev, N. I. *Nano Lett* **2010**, *10*, 3250-3252.

(3) Kawata, S.; Ono, A.; Verma, P. *Nat Photonics* **2008**, *2*, 438-442.

(4) Arnold, M. D.; Blaikie, R. J. *Opt Express* **2007**, *15*, 11542-11552.

(5) Hafner, J. H.; Mayer, K. M. *Chem Rev* **2011**, *111*, 3828-3857.

(6) Kealley, C. S.; Arnold, M. D.; Porkovich, A.; Cortie, M. B. *Sensor Actuat B-Chem* **2010**, *148*, 34-40.

(7) Kreibig, U.; Vollmer, M. *Optical Properties of Metal Clusters*; Springer-Verlag, 1995; Vol. 25.

(8) de Abajo, F. J. G. *J Phys Chem C* **2008**, *112*, 17983-17987.

(9) Blaber, M. G.; Arnold, M. D.; Ford, M. J. *J Phys Chem C* **2009**, *113*, 3041-3045.

(10) Arnold, M. D.; Blaber, M. G. *Opt Express* **2009**, *17*, 3835-3847.

(11) Blaber, M. G.; Arnold, M. D.; Ford, M. J. *J Phys-Condens Mat* **2010**, *22*, 143201.

(12) Sarychev, A.; Shalaev, V. *Electrodynamics of Metamaterials*; World-Scientific: Singapore, 2007.

(13) Fidder, H.; Knoester, J.; Wiersma, D. A. *J Chem Phys* **1991**, *95*, 7880-7890.

(14) Markel, V. A.; Sarychev, A. K. *Phys Rev B* **2007**, *75*, 085426.

(15) Auguie, B.; Barnes, W. L. *Opt Lett* **2009**, *34*, 401-403.

(16) Halas, N. J.; Lal, S.; Chang, W. S.; Link, S.; Nordlander, P. *Chem Rev* **2011**, *111*, 3913-3961.

(17) Arnold, M. D.; Blaber, M. G.; Ford, M. J.; Harris, N. *Opt Express* **2010**, *18*, 7528-7542.

(18) Park, S. Y.; Stroud, D. *Phys Rev B* **2004**, *69*, 125418.

(19) Bergman, D. J. *Phys Rev B* **1979**, *19*, 2359-2368.

(20) Mackowski, D. W. *J Opt Soc Am A* **1994**, *11*, 2851-2861.

(21) Harris, N.; Arnold, M. D.; Blaber, M. G.; Ford, M. J. *J Phys Chem C* **2009**, *113*, 2784-2791.

(22) Weaver, J. H.; Frederikse, H. P. R. Optical Properties of Selected Elements. In *CRC Handbook*; CRC, 2001.

(23) McMahon, J. M.; Gray, S. K.; Schatz, G. C. *Nano Lett* **2010**, *10*, 3473-3481.

Figure 1: Geometry of the system to be simulated together with the excitation conditions.

Figure 2: Example of spreading of eigenvalues and mode weight with disorder. These chains had N=9 particles, average gap fraction of f=0.1, and random configurations characterized by disorder with standard deviation 0.1 times the gap. The black circles indicate the modes of the ordered chain, and the dots indicate modes of disordered chains. Only the lowest order modes are shown for clarity, with the collective dipole mode on the left (j=1). Note the much stronger spread of weight than depolarization.

Figure 3: Example of extinction for potassium spheres with modes corresponding to those in the previous figure – short wavelength peaks have been omitted for clarity. The black circles indicate the modes – the ordering in wavelength space is reversed compared to depolarization so the collective dipole (j=1) is now on the right. The black line is the extinction for the ordered chain, while the blue line is the mean extinction for the ensemble. The red background shows the statistical distribution – note particularly the high degree of skew around the dipole peak.

Figure 4: Comparison of relative mode-shifts with (red circles labeled "VSH") and without (blue dots labeled "multimode") retardation, showing that the scaling is very similar and thus retardation is not significant. In this example the gap fraction is f=0.04, and the retarded results are for Au spheres with a=7.5nm. The relative shift is shown in terms of the disordered peak permittivity ε^{dis} compared to the ordered peak permittivity ε^{ord}. These results are directly related to the non-retarded mode parameter S, but this relationship is less rigorous when retardation is included.

Figure 5: Average red-shift ($-\langle\delta S\rangle$) and damping ($-\langle\delta A\rangle$) of the collective dipole mode (j=1) as a function of disorder (σ/g) and coupling strength. (a) The mode shift is quadratic with

disorder σ/g, even at strong couplings (f<1). (b) The shift decays nearly exponentially with reduced coupling (increasing f). The asymptotic models described by Eq (7) and (8) are overlaid at small f (dashed) and large f (dash-dotted) respectively. Relative damping of the dipole strength A increases with increasing disorder (c) but decreases with increasing coupling (d).

Figure 6: Standard deviation (left) and skew (right) of the red-shift (top) and damping ratios (bottom), as a function of disorder at different gap fractions, for the collective dipole mode (j=1). Note that the normalized deviation (a & c) is quite significant compared to the mean value shown in the previous Figure. Further, the skew is strong and increases strongly with disorder, but is nearly independent of gap fraction (b & d). Hence, when considering ensemble results it is important to remember that individual results can vary widely from the mean, and that the distribution is strongly skewed.

Figure 7: Fractional contributions to perturbation of the collective dipole mode (j=1) as a function of disorder and coupling strength. Second order clearly makes a significant contribution, and surpasses the first order for strong couplings when gap-fraction f<0.5 (a). Higher orders are negligible, especially for weak disorder (b).

Figure 8: Average relative shift of the main peak wavelength λ_p for various metals (Ag, Al, Au, K) as a function of coupling strength (inversely related to the gap fraction f). The shift of the wavelength is quite small, especially for Au (c), but it increases with both coupling and disorder. The dashed line shows the shift of the ensemble for the largest disorder, which is very similar to the average shift of individual configurations.

Figure 9: Average relative broadening of the main peak width Δ_p for various metals (Ag, Al, Au, K) as a function of coupling strength (inversely related to the gap fraction *f*). There is some broadening at moderate coupling, but this is less pronounced for Au (c). The dashed line shows the broadening of the ensemble for the largest disorder, which is substantially stronger for K (d) at strong coupling.

Figure 10: Average change of the main peak extinction C_p for various metals (Ag, Al, Au, K) as a function of coupling strength (inversely related to the gap fraction *f*). The extinction of chains of ideal metals such as K is damped by disorder (d) whereas poorer metals such as the commonly used Au are much more robust (c). The dashed line shows the change in peak extinction of the ensemble, which shows significantly increased damping for K (d).

(Figure 1)

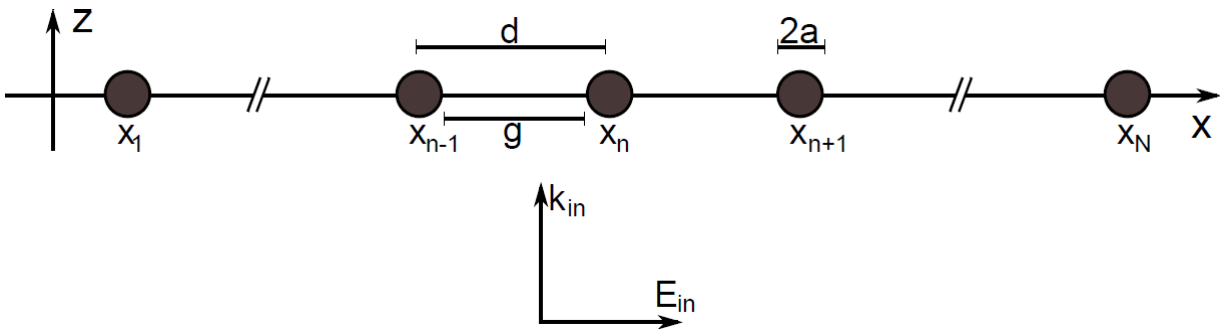

(Figure 2)

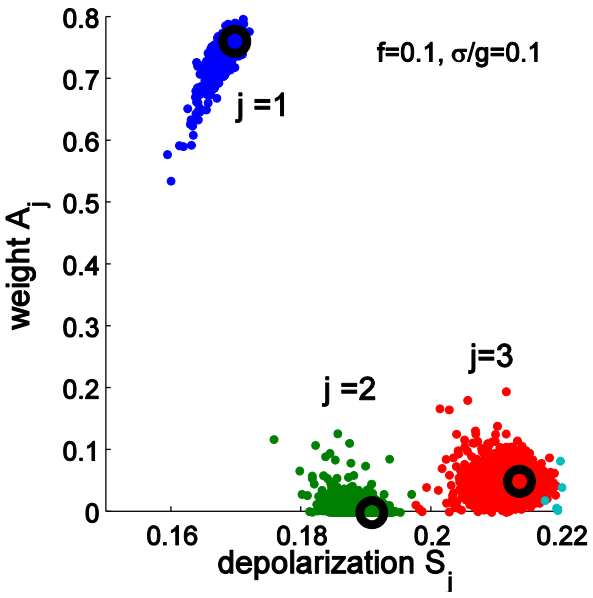
f=0.1, σ/g=0.1
j =1
j =2
j=3
weight A_j
depolarization S_i
0.8
0.7
0.6
0.5
0.4
0.3
0.2
0.1
0
0.16
0.18
0.2
0.22

(Figure 3)

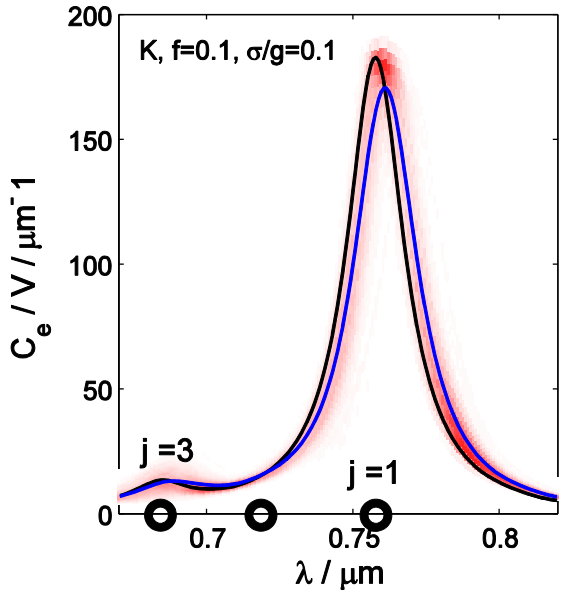

(Figure 4)

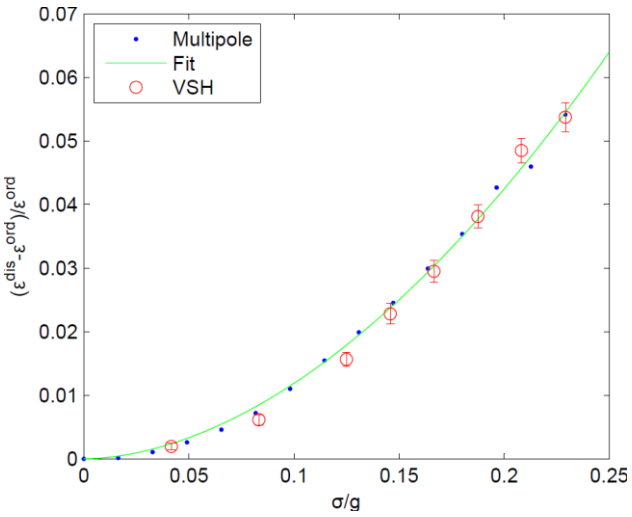
Multipole
Fit
VSH
0.07
0.06
0.05
0.04
0.03
0.02
0.01
0
0
0.05
0.1
0.15
0.2
0.25
σ/g
$\rho_{uo}^3/(\rho_{uo}^3-\varepsilon_{slip}^3)$

(Figure 5)

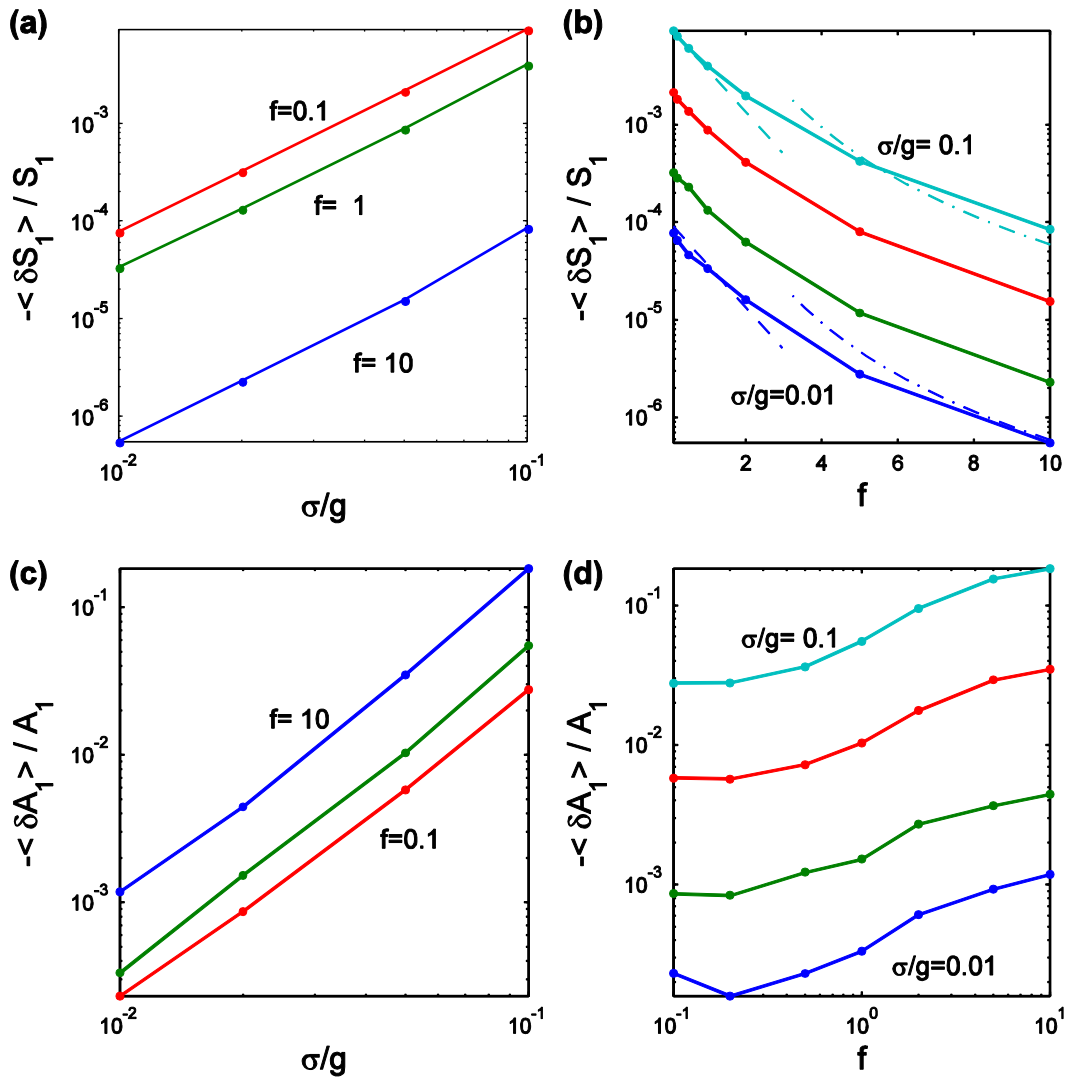

(Figure 6)

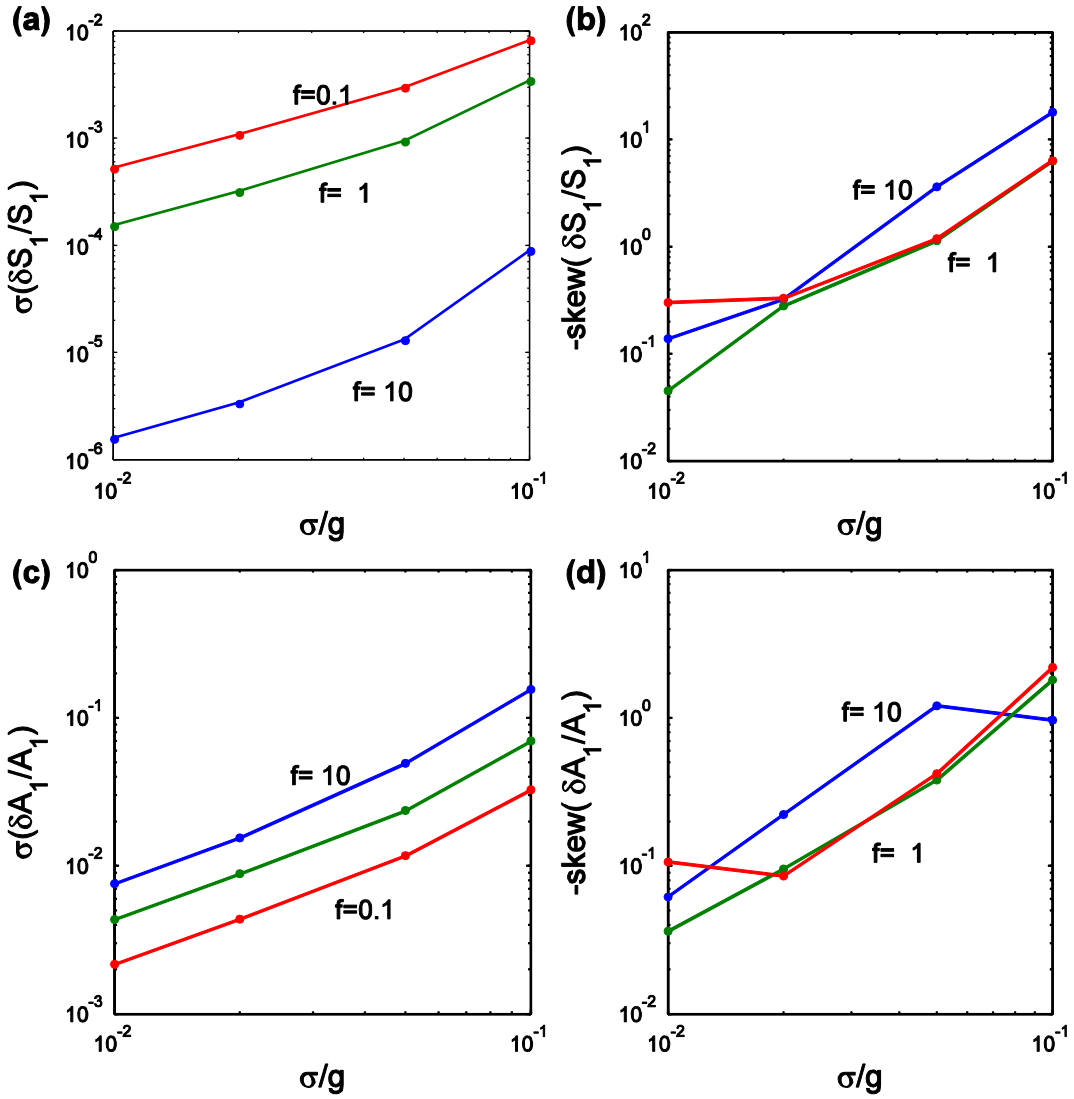
(a)
σ(δS1/S1)
f=0.1
f= 1
f= 10
σ/g
(b)
-skew(δS1/S1)
f= 10
f= 1
σ/g
(c)
σ(δA1/A1)
f= 10
f=0.1
σ/g
(d)
-skew(δA1/A1)
f= 10
f= 1
σ/g

(Figure 7)

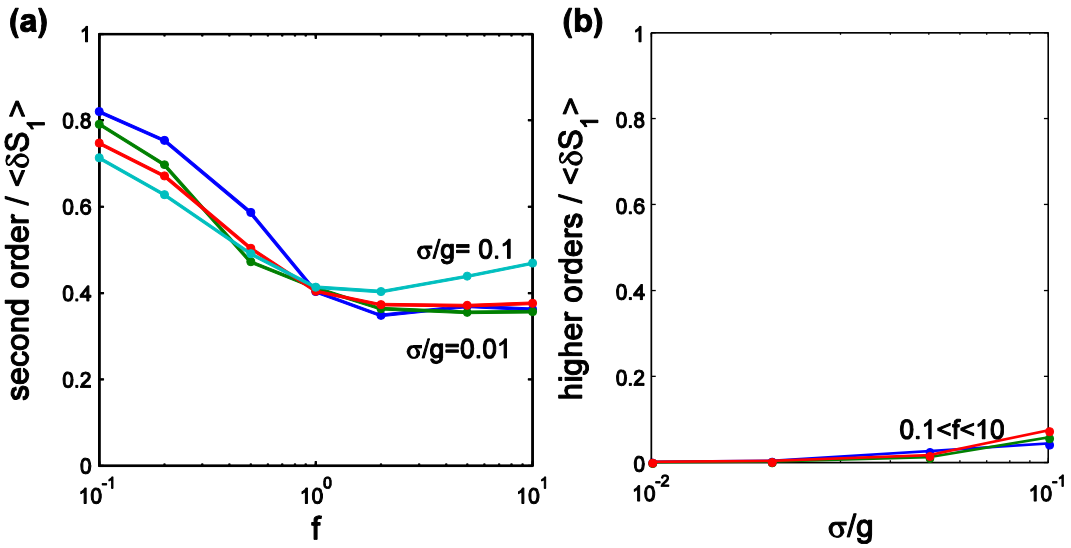

(Figure 8)

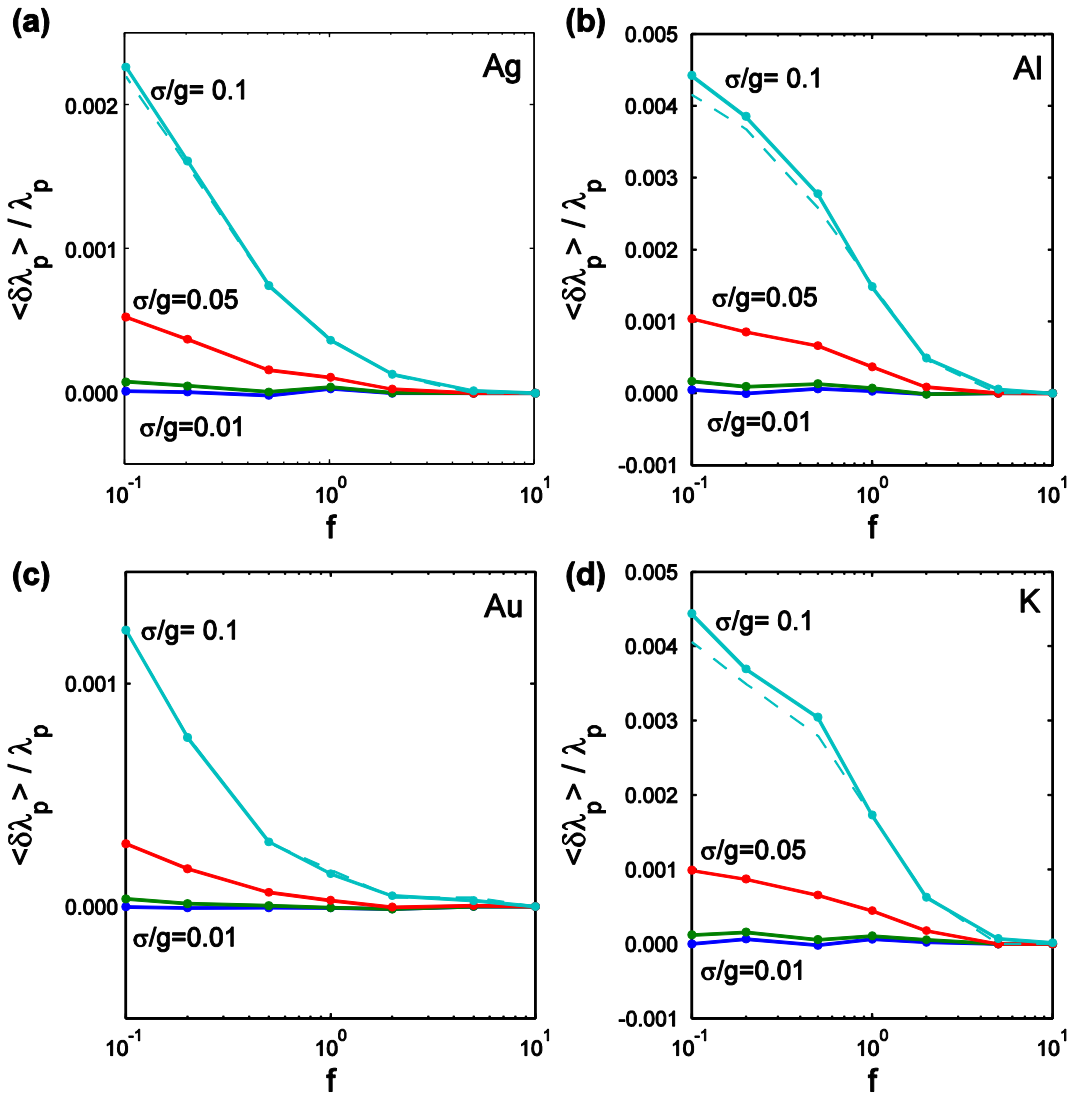
(a)
Ag
σ/g= 0.1
σ/g=0.05
σ/g=0.01
<δλp> / λp
f
(b)
Al
σ/g= 0.1
σ/g=0.05
σ/g=0.01
<δλp> / λp
f
(c)
Au
σ/g= 0.1
σ/g=0.01
<δλp> / λp
f
(d)
K
σ/g= 0.1
σ/g=0.05
σ/g=0.01
<δλp> / λp
f

(Figure 9)

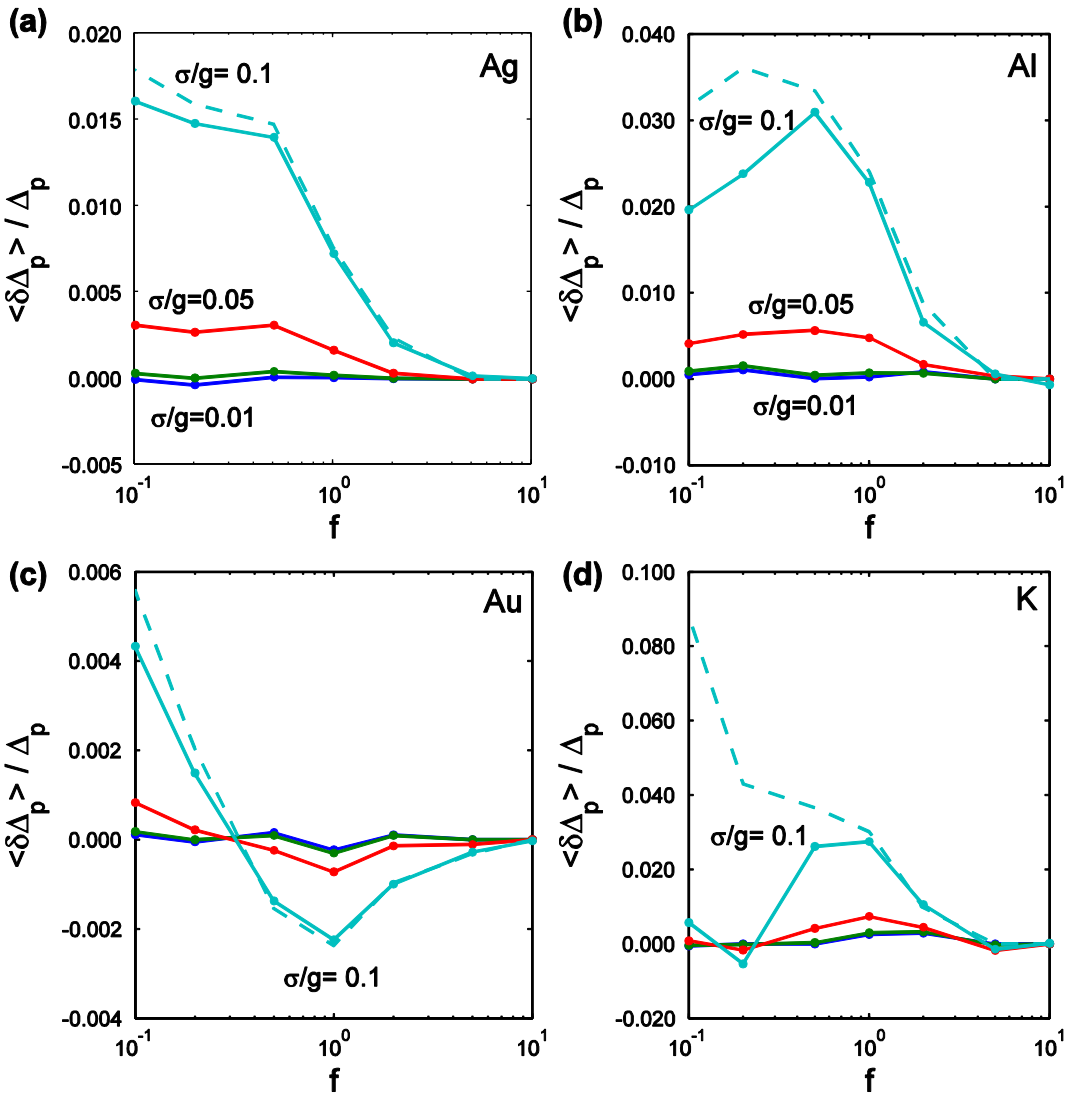
(a)
Ag
σ/g= 0.1
σ/g=0.05
σ/g=0.01
<δΔp> / Δp
f
(b)
Al
σ/g= 0.1
σ/g=0.05
σ/g=0.01
<δΔp> / Δp
f
(c)
Au
σ/g= 0.1
<δΔp> / Δp
f
(d)
K
σ/g= 0.1
<δΔp> / Δp
f

(Figure 10)

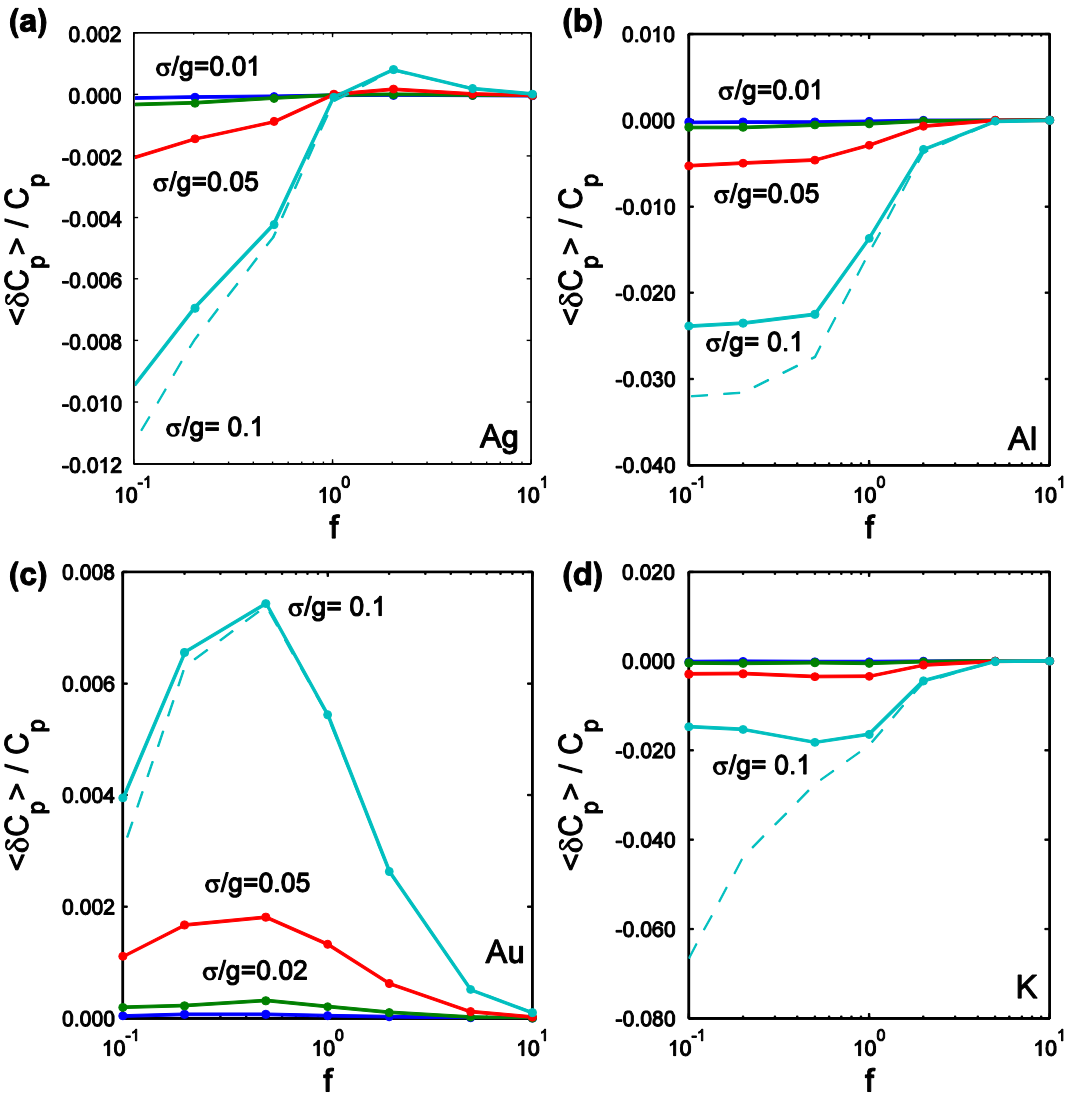
(a)
σ/g=0.01
σ/g=0.05
σ/g= 0.1
Ag
<δC_p > / C_p
f
(b)
σ/g=0.01
σ/g=0.05
σ/g= 0.1
Al
<δC_p > / C_p
f
(c)
σ/g= 0.1
σ/g=0.05
σ/g=0.02
Au
<δC_p > / C_p
f
(d)
σ/g= 0.1
K
<δC_p > / C_p
f

(TOC Image)

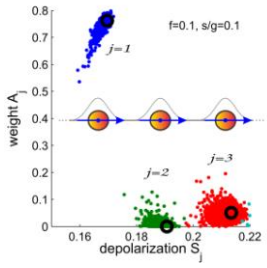
f=0.1, s/g=0.1
j=1
j=2
j=3
weight A_j
depolarization S_j
0.8
0.7
0.6
0.5
0.4
0.3
0.2
0.1
0
0.16
0.18
0.2
0.22